Time evolution of many-body localized systems in two spatial dimensions

A. Kshetrimayum,[1,2] M. Goihl,[1] and J. Eisert [1,2]

[1]*Dahlem Center for Complex Quantum Systems, Freie Universität Berlin, 14195 Berlin, Germany*
[2]*Helmholtz Center Berlin, 14109 Berlin, Germany*

Many-body localization is a striking mechanism that prevents interacting quantum systems from thermalizing. The absence of thermalization behavior manifests itself, for example, in a remanence of local particle number configurations, a quantity that is robust over a parameter range. Local particle numbers are directly accessible in programmable quantum simulators, in systems of cold atoms, even in two spatial dimensions. Yet, the classical simulation aimed at building trust in quantum simulations is highly challenging. In this work, we present a comprehensive tensor network simulation of a many-body localized systems in two spatial dimensions using a variant of an infinite projected entangled pair states algorithm. The required translational invariance can be restored by implementing the disorder into an auxiliary spin system, providing an exact disorder average under dynamics. We can quantitatively assess signatures of many-body localization for the infinite system: Our methods are powerful enough to provide crude dynamical estimates for the transition between localized and ergodic phases. Interestingly, in this setting of finitely many disorder values, which we also compare with simulations involving noninteracting fermions and for which we discuss the emergent physics, localization emerges in the interacting regime, for which we provide an intuitive argument, while Anderson localization is absent.

I. INTRODUCTION

While generic ergodic systems are expected to thermalize under closed system evolution [1–3], constituting their own heat bath, systems that exhibit many-body localization (MBL) are a robust exception to this paradigm [3–6]. Such systems do equilibrate, but they retain too much memory of the initial condition so that the time-averaged states could be described by a thermal ensemble, due to *localization*. The localization gives rise to quasilocal constants of motion in real space [6–8], which need to be included in an equilibrium ensemble, leading to a nonthermal equilibrium state. MBL can be seen as an intricate generalization of the well-known Anderson localization in which disorder and interactions come together. Since its discovery in the early years of this millennium [4], a plethora of theoretical works followed elucidating the rich and multifaceted phenomenology of MBL in one spatial dimension, ranging from a logarithmic growth of entanglement [9–12] over slow information propagation [13,14] to an *area law* for the entanglement entropy [15] for highly excited eigenstates [16,17]. Experimental realizations have followed for MBL systems in one spatial dimension [18–21], corroborating some of the phenomenology.

In two spatial dimensions, MBL is significantly less understood. Experiments with ultracold atoms have been pursued [18], showing localization under precisely controlled conditions. Yet, much of the phenomenology is less clear—to the extent that it has been suggested that MBL may be unstable altogether and that ergodicity could eventually be restored,

albeit on very long time scales [22,23]. Such assessments are made difficult by numerical treatments being excessively challenging [24]. Steps have been taken in the numerical analysis: Ref. [25] constructs a two-dimensional cellular automaton, further seminal works discuss finite [26] and infinite [27] disordered systems numerically, while Ref. [28] targets weakly interacting systems of finite sizes. Exact diagonalization limits discussions to either noninteracting or extremely small systems. Tensor network approaches are immensely challenged by the entanglement buildup, even if this is slower compared to ergodic systems [9–11]. Still, given the unfavorable scalings of bond dimensions to faithfully present quantum states as tensor networks, this still gives rise to a challenging and intricate state of affairs.

In this work, we present an alternative take on the problem of simulating time evolution of many-body localized two-dimensional quantum systems. We discuss the physics of infinite two-dimensional systems featuring discrete disorder using infinite projected entangled pair states (iPEPS), building upon a methodology recently introduced in Refs. [27,29], in turn building upon Ref. [30]. The translational invariance inherent in this ansatz will be restored here by exploiting a quantum dilation that embodies the classical disorder in giving rise to exact disorder averages, an ansatz suggested some time ago [30] and recently implemented for disordered two-dimensional systems [27] in a proof-of-principle methodological study, using a different iPEPS update from the one simple update employed here. While the so-called full update is known to be more accurate for ground-state simulations for

the same bond dimension, whenever possible, it is an interesting observation in its own right that simple updates—more resource-efficient procedures—turn out to be significantly more stable in time evolution algorithms, as experience with numerical procedures has shown [27] and is convincingly confirmed in this work, presumably for being better able to reflect local changes in time evolution. That is to say, our scheme that we employ here is more stable, resource-efficient, and provides better control over the dynamics. For this reason, we have been able to achieve the longest available times in 2D dynamics following a global quench for strongly interacting systems ($t = 3J$) to date in the thermodynamic limit, thanks to the disorder present.

We argue that while disorder averages are comparably feasible in one-dimensional studies, it is a two-dimensional setting, for which quantum dilations capture classical disorder averages, that is particularly practical and relevant. Intriguingly, the implementation of programmable discrete disorder can avoid the issue of ergodic bubbles right from the outset [22,23], sidelining the issue of stability of many-body localization in higher dimensions. Such an implementation of discrete disorder gives rise to a situation that is already intriguing in the noninteraction case reflecting Anderson localization. Building upon early work [31], there has been a recent revitalized interest in rigorous studies of Anderson localization for instances of discrete disorder in the absence of interactions [31,32,32–35]. These rigorous results prove the existence of localization in specific regimes of discrete disorder discussed in more detail later. Interestingly, however, within the settings considered here we do not find signatures of dynamical localization on the time scales considered. For this phenomenon, we provide an explanation in terms of discrete disorder leading to an effective hopping problem on every level. We augment this argument by numerical simulations of a finite noninteracting system using exact diagonalization, which are further supplemented by iPEPS. In the presence of interactions, we find signatures of localization in the local particle number and suitable Renyi entropies, entering a highly exciting new physical regime, which we discuss in great detail.

We will start by discussing the underlying paradigmatic model that is at the heart of our analysis, and then turn to discussing the numerical methods we make use of and develop to study the disordered model (both the free fermions and iPEPS). We present the results for the noninteracting as well as the interacting instance of the Hamiltonian. In Sec. III, we will specifically describe how the translationally invariant iPEPS can be used to realize disorder by introducing dilations. Section IV includes a discussion of the absence of Anderson localization and numerical evidence supporting it from two independent techniques. We then discuss the results for the evidence of many-body localization in the interacting case. Based on the particle imbalance $\mathcal{I}$, which we compute for different configurations of the parameters, we are able to estimate a crude dynamical phase diagram of MBL in two dimensions. The critical disorder strength is found to be $h \approx 6$ with at least four levels of disorder. We close in Sec. V by summarizing the results and giving an outlook for future work including possible experimental realizations in state-of-the-art analog quantum simulators.

II. MODEL AND LOCALIZATION MEASURE

The model we focus on is the spin-1/2 XXZ-Hamiltonian on a square lattice with disordered fields

$$H = \sum_{\langle i,j \rangle} \left(S_i^x S_j^x + S_i^y S_j^y + \Delta S_i^z S_j^z \right) + \sum_i h_i S_i^z, \quad (1)$$

where S^x, S^y, and S^z are the different Pauli spin operators associated with a particular site. Δ is the strength of the anisotropy, which we choose to be either $\Delta = 0$ or 1, which toggles many-body interactions. The value of the magnetic field at a particular site is given by h_i. Usually h_i are drawn randomly from a continuous interval $[-h, h]$ for each site in the lattice, but we will soon turn to other discrete probability measures.

The essence of MBL is the localization of its constituent particles leading to a breakdown of conductance [4] and thermalization [18] despite the presence of many-body interactions. A proxy for these effects is the local particle number dynamics following a quench from a particle imbalanced initial state. We consider a Néel state vector of the form

$$|\psi_0\rangle_p = |\uparrow, \downarrow, \uparrow, \downarrow, \ldots, \rangle. \quad (2)$$

When subjected to the Hamiltonian evolution of a thermalizing Hamiltonian, the local particle imbalance quickly evens out and evolves toward a homogeneous particle distribution [36]. However, if the Hamiltonian localizes the constituent particles, the initial particle imbalance will be measurable for very long times [18]. We stress that the observation of a remaining particle imbalance for a finite time window does not give information about the "genuine" quantum phase the system is actually in, as for long times the system can still thermalize [22,37,38]. However, even localization for short times can be relevant for experimental realizations [18] and practical applications such as quantum memories [39].

III. SETTING

Usually, when working with disordered systems numerically, in order to obtain disorder averaged quantities, simulations need to be run multiple times, and the disorder average of the expectation values of the local observables are then calculated. In this case, a single realization of a system is not translationally invariant and hence finite. There is another technique of realizing disordered models that circumvents the above finite-size effects and running the simulations multiple times to obtain statistics for the disorder average. The method makes use of additional auxiliary dilation spaces at every site whose spin states are in superposition. Upon tracing out this degree of freedom, one obtains the exact disorder averages, as introduced in Ref. [30]. Since the combined system is translationally invariant, we can access the thermodynamic limit using translationally invariant algorithms. This is the approach we will be taking in this work. We will describe the algorithm used in our setting in more detail in the subsequent sections.

A. Setup for iPEPS

Projected entangled pair states (PEPS) are the generalization of matrix product states to higher dimensions [40,41].

Similar to its one-dimensional counterpart, PEPS target the physically relevant corner of the Hilbert space that is distinguished by its low entanglement content while representing a quantum state in higher dimensions [42–44], which are of physical interest. One of the many advantages of such tensor network techniques is that they enable us to directly study systems in the thermodynamic limit, thereby overcoming finite-size effects, which one would often encounter using techniques such as exact diagonalization. In this context, the infinite projected entangled pair states (iPEPS) [45] have become the state-of-the-art numerical tool in simulating two-dimensional systems. They have been known to provide excellent variational ground-state energies, in some instances even outperforming the state-of-the-art quantum Monte Carlo calculations [46]. The success of iPEPS lies beyond simulating two-dimensional simple cubic lattices. iPEPS have found applications in finding ground states of frustrated systems [47–49] and realistic materials [50–52]. They have also been used to describe thermal states in 2D [53–56] as well as steady states of dissipative systems [57,58]. While most of these works target the fixed points of the model, it is also possible, in principle, to use iPEPS for studying the dynamics of a system. This is limited to only short time scales due to the fast growth of entanglement. The situation is true for all Tensor networks and even more severe for two-dimensional systems, further limiting the accessible time scales [27,59]. In this work, we will use iPEPS to study the dynamics of the XXZ-Hamiltonian [Eq. (1)] in the presence of disorder and look for signatures of localization in different regimes of the anisotropy Δ, as well as the number of discrete levels d_A of disorder.

In our setting, we exploit what can be called "quantum parallelism" to realize disorder in our translationally invariant system in the thermodynamic limit, as first proposed in Ref. [30] and realized in one- [29,60] and two- [27] dimensional disordered systems. In essence, the method implements discrete disorder using auxiliary spin-S systems for otherwise translationally invariant Hamiltonians. There is one of these auxiliary spaces for each real space site, and they are prepared in a superposition state of all their spin states. By adding another term to the Hamiltonian that projects these values onto the real space, we obtain discrete disorder landscapes. When calculating expectation values of observables, the states of the auxiliary space actually conveniently implement the disorder average over all possible disorder realizations. We will now break down this procedure into three important steps in order to implement this type of disorder.

(i) *Initialization:* We initialize our physical state vector $|\psi_0\rangle_p$ as a product that is easy to prepare experimentally, more specifically the Néel state, i.e.,

$$|\psi_0\rangle_p = |\uparrow, \downarrow, \uparrow, \downarrow, \ldots\rangle. \qquad (3)$$

For our simulations, we have chosen an iPEPS with a two-site unit cell and a checkerboard pattern as shown in Fig. 1(a). This is sufficient to realize the configurations of interest. We also initialize the auxiliary state in a product state of equal superposition state vector $|+\rangle$, i.e.,

$$|\psi_0\rangle_a = |+, +, +, \ldots\rangle. \qquad (4)$$
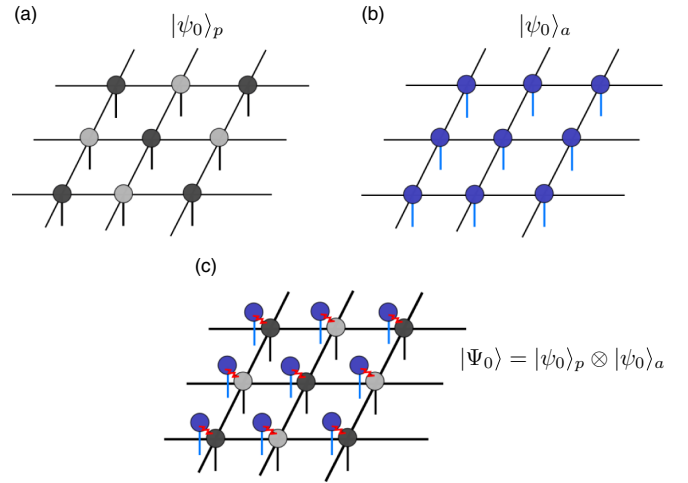

FIG. 1. Initial state expressed in terms of iPEPS for (a) the physical state vector $|\psi_0\rangle_p$, which is a Néel state; (b) the auxiliary state vector $|\psi_0\rangle_a$, which is a product of equal superposition states; and (c) the overall initial state vector $|\Psi_0\rangle$, which is the tensor product of the previous two states. The red patterns correspond to the classical interaction between the physical and the auxiliary states, which is required for introducing the disorder. All three states are iPEPS with bond dimension $D = 1$ and the lattice extends indefinitely in all directions. A choice of a two-site unit cell in a checkerboard pattern is enough to exactly represent this configuration.

For a spin-S system, this superposition is given by $|+\rangle = (2S + 1)^{-1/2}(\sum_s |s\rangle)$, where s are the allowed spin states. Hence, the number of discrete values that our disordered field takes is $2S + 1$, where S is the spin of the auxiliary space. Thus, the number of discrete levels of disorder, which we refer to as d_A, is two for a spin-1/2, three for a spin-1 auxiliary system, and so on. We then take the tensor product of the initial physical state vector and the initial auxiliary state vector and define this to be our overall initial state from where we start quenching, i.e.,

$$|\Psi_0\rangle = |\psi_0\rangle_p \otimes |\psi_0\rangle_a, \qquad (5)$$

where $|\Psi_0\rangle$ is a product state vector and hence an iPEPS with bond dimension $D = 1$. This completes the initialization protocol, which we also illustrate in Fig. 1.

(ii) *Quench:* Once our initial state has been prepared, we perform the real-time evolution of our disordered Hamiltonian. For this, the original Hamiltonian in Eq. (1) needs to be rewritten as

$$H = \sum_{\langle i,j \rangle} \left(S_{i_p}^x S_{j_p}^x + S_{i_p}^y S_{j_p}^y + \Delta S_{i_p}^z S_{j_p}^z \right) + h \sum_i S_{i_p}^z S_{i_a}^z, \qquad (6)$$

where the first term of the Hamiltonian is the sum over all the nearest-neighbor physical sites. The second term couples each physical spin with its auxiliary spin, but there is no coupling between different sites. This term projects the disorder contained in the auxiliary space onto the physical state using the local $S_{i_p}^z S_{i_a}^z$ coupling. $S_{i_a}^z$ is defined such that the values of the disordered fields are taken from a fixed interval $[h, -h]$ with uniform distribution. Thus, for d_A the values will be h and $-h$, for $d_A = 3$ they would be $h, 0$, and $-h$, and so on. We will study the effect of disorder as we increase the dimension

of the auxiliary system d_A thereby allowing more levels of disorder configurations. We use the simple update [61] to do a real-time evolution of our modified Hamiltonian starting from the initial state vector $|\Psi_0\rangle$,

$$|\Psi(t)\rangle = e^{-iHt}|\Psi_0\rangle. \qquad (7)$$

This update scheme is not only efficient, but is also more stable while dealing with such nonequilibrium problems [27]. This might be due to the fact that unlike the full update technique, the simple update does not require us to compute the ill-conditioned norm tensor at every step.

(iii) *Readout:* Once we have generated the state vector $|\Psi(t)\rangle$ using the procedure described above, we can compute the expectation values of suitable local observables. Such expectation values are already the exactly disorder averaged expectation value of all the possible configurations by construction. This can be easily seen from the following calculation:

$$\begin{aligned}
\mathbb{E}\langle\hat{O}(t)\rangle &= \langle\Psi(t)|\hat{O}|\Psi(t)\rangle \\
&= \langle\Psi_0|e^{iHt}\hat{O}e^{-iHt}|\Psi_0\rangle \\
&= ({}_a\langle\psi_0| \otimes {}_p\langle\psi_0|)e^{iHt}\hat{O}e^{-iHt}(|\psi_0\rangle_p \otimes |\psi_0\rangle_a).
\end{aligned} \qquad (8)$$

The on-site expectation value is calculated at the physical site as the auxiliary sites are traced out. We use an instance of a CTMRG algorithm [62,63] for this purpose. We also use the same effective environment to compute the different Renyi entropies of the reduced density matrices.

Thus, the above procedure circumvents the need to have finite systems to realize disordered systems, at the same time avoiding the need for multiple simulations for different disorder configuration and taking their average.

B. Setup for noninteracting fermions

In addition to the iPEPS simulations described above, we have also run some free fermionic calculations reminiscent of the noninteracting case $\Delta = 0$ in a finite system (note that the mapping is not exact due to the presence of Jordan-Wigner strings in two spatial dimensions). Because the dynamics is only governed by the single-particle sector, systems of size 40×40 are perfectly accessible. Moreover, we can implement continuous disorder for these simulations. In accordance with our iPEPS simulation, we again consider a Néel initial state and evolve it in time. We measure the particle number on even and odd sites as a measure of localization [18] as described above. Here, we are in principle not restricted to any final time, but we since we are interested in comparing the results to the iPEPS simulations, we evolve up to a few tunneling times by integrating Schrödinger's equation. Additionally, we can access the single-particle eigenstates and single-particle eigenenergies of these systems via exact diagonalization, which we employ to calculate the inverse participation ratio, another measure of localization.

IV. RESULTS

In this section, we present results for the noninteracting case $\Delta = 0$. In this regime, it is possible to solve larger two-dimensional systems exactly in the single-particle space. It

has been rigorously established that one- and two-dimensional systems localize for continuous disorder [64–66]. For discrete disorder the situation is more subtle. In fact, seminal work has solved the long-standing puzzle regarding whether localization occurs in the first place in one spatial dimension, showing that it does in fact occur [31]: Interestingly, for one spatial dimension, any probability measure that has support for more than a single point will lead to the Hamiltonian having a pure point spectrum and exponentially decaying eigenfunctions and hence localization, even though bounds to localization lengths are implicit. These results are compatible with rigorous insights into dynamical localization for suitable random Schrödinger operators [33]. In higher dimensions, slightly weaker statements are shown, basically for sufficiently large disorder [31], for disorder with sufficiently large numbers of discrete levels of disorder [32], or for parts of the spectrum [34,35]. These results apply equally well to our situation of noninteracting fermionic systems.

The dynamics of the particle number for even and odd sites in the noninteracting fermionic case is shown in Fig. 2. Here, we present results for three disorder strengths ($h = 4, 10, 100$) and two kinds of disorder: Continuous disorder is shown in red shades and a three-level discrete (spin-1) disorder is shown in blue shades. The two curves plotted depict the particle number for odd and even sites, respectively. Furthermore, we plot data obtained for the infinite system with the iPEPS code in black. This serves a more qualitative purpose, however, since the plots shown are for iPEPS with fixed bond dimension $D = 4$ and therefore we should be careful in making a one-to-one comparison with the exact diagonalization results quantitatively. For $h = 4$, we find that the initial imbalance evens out on the time scales considered. There is no apparent difference for the two disorder models considered. This apparent lack of localization is by no means incompatible with the above proven localization: On the one hand, in two spatial dimensions (unlike in one spatial dimension), the disorder has to be sufficiently strong to encounter localization. More importantly, on the other hand, the figure of merit applied will only encounter localization on the spatial extent of single lattice sites. Hence, the absence of localization for the magnetization is compatible with localization for longer localization lengths. In fact, the machinery developed here gives rise to a tool to explore this rich physics for discrete disorder in higher spatial dimensions.

For $h = 10$, we find that a first signature of localization for the time scales considered as a weak imbalance—signified by a gap between the two curves—remains. When comparing the two disorder models, we already see a hint toward an observation that will become more clear in the strongly disordered case. The continuous disorder results in a slightly larger gap. When we set $h = 100$, there is a large gap for the continuous disorder model, but only a small one for the discrete disorder model. The simulation for the infinite system agrees very well with the finite calculations for $t < 1$. It furthermore suggests that with increasing system size, the gap closes completely. Moreover, we find that increasing the levels of the discrete model results in a larger gap (data not shown).

To complement this analysis, we also look at the single-particle energy spectrum to understand the influence of the discrete disorder and why dynamical localization may not
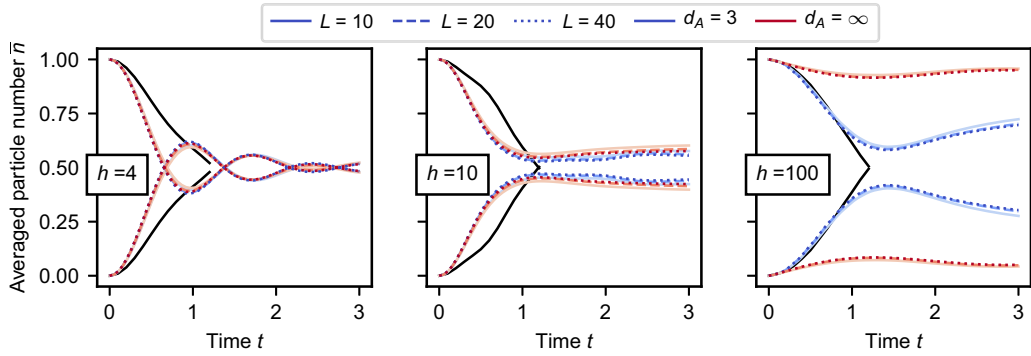
FIG. 2. Averaged local particle number for even and odd sites in a free fermionic model for system sizes $L = 10, 20, 40$ (markers). Averages are taken over 100 realizations. Blue shades are for discrete disorder (spin-1) and red shades for continuous disorder. The black dotted lines are iPEPS results for an infinite system. They are presented only to give a qualitative prediction of how the results using the free fermion simulation will change in the thermodynamic limit. A one-to-one quantitative comparison should not be made with the iPEPS results, since the plot shown is for $D = 4$. However, the agreement between the two techniques is striking for the large disorder case $h = 100$ since the entanglement growth is much slower here and the bond dimension does not play much of a role within the time scale presented here.

occur for the observed times in the discrete disorder model. In Fig. 3, we plot the spectra for both models at high disorder $h = 100$. We find that the spectrum for the continuous disorder is apparently still continuous. When discrete disorder with s many levels is used, the spectrum is decoupled in s blocks that have a weak bending caused by the hopping terms. This is compatible with the following intuitive explanation, which is furthermore in line with the above rigorous findings: Since the energy gaps between the levels are very large, the system effectively largely decouples into sites of the same disorder strength. Depending on the position of the next site with the same disorder value, the hopping strength will change, but essentially the physics boils down to a hopping problem with a high coordination number and random hopping strengths. This implies that for long times, the system will evolve toward a homogeneous state.

To give more substance to this heuristics, we consider the inverse participation ratio (IPR) defined as

$$I_{|E_k\rangle} = \sum_i |\langle i|E_k\rangle|^4, \quad (9)$$

where $|i\rangle$ is a lattice site vector and $|E_k\rangle$ is the eigenvector with corresponding energy E_k. This provides an estimate of
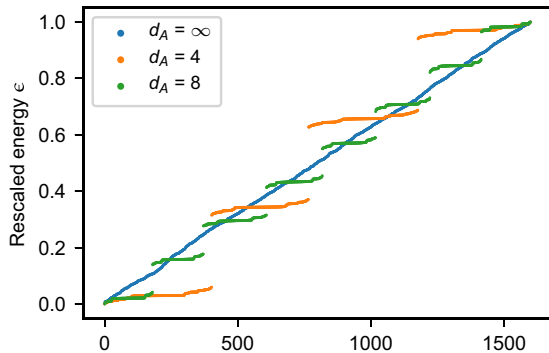
the localization of the eigenvectors in the following sense. If $|E_k\rangle$ only has support on a single lattice site, its IPR is unity. If, in contrast, $|E_k\rangle$ has support on all lattice sites, the IPR will be $1/L^2$. We consider a cumulative IPR for energy segments. This means that we rescale the spectrum according to

$$\epsilon(E) = \frac{E - E_{\min}}{E_{\max} - E_{\min}}, \quad (10)$$

such that $0 \leqslant \epsilon \leqslant 1$. We then sum the IPR for all states in rescaled energy intervals of size 0.05. The results are displayed in Fig. 4. For low disorder $h = 4$ (squares), the IPR is approximately the same for all three types of disorder. For $h = 10$ (circles), we see that at the ends of the spectrum, the IPR is lower for fewer levels of disorder. When considering the case of high disorder $h = 100$, there is a strong qualitative difference for the models. The continuous disorder results in a very high IPR throughout the full spectrum. Not only is

FIG. 3. Single-particle spectrum for the Anderson model with discrete and continuous disorder for $h = 100$ averaged over 100 realizations.
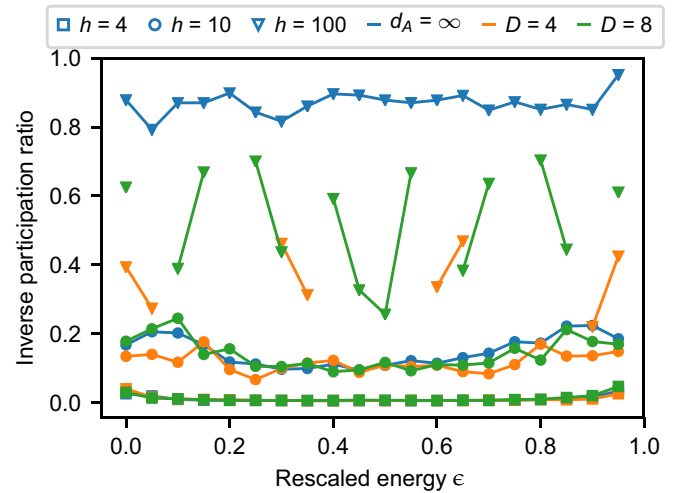

FIG. 4. Cumulative inverse participation ratio for the Anderson model with discrete and continuous disorder for different disorder strengths. Lines are guides to the eye. When the energy levels for a certain value ϵ are not populated, no line is drawn.
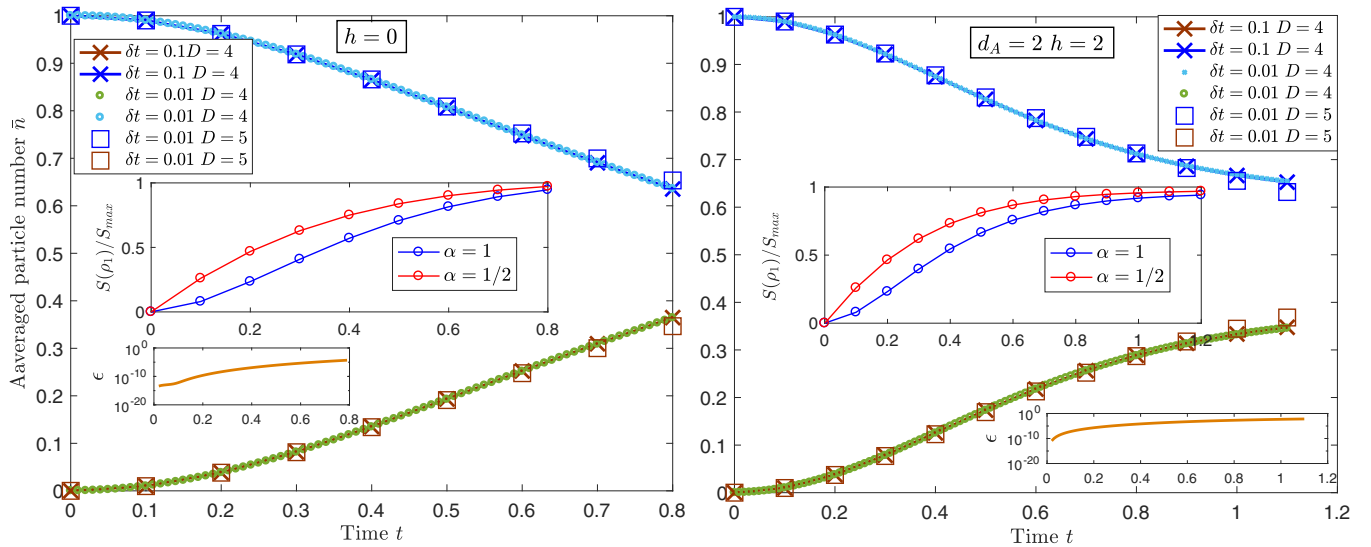
FIG. 5. Real-time evolution of the Heisenberg Hamiltonian starting from a Néel state. Left: Expectation value of the particle number as a function of time for the two different sites for the case with no disorder $h = 0$. Big inset: Renyi entropies of the reduced density matrix of one site as a function of time for $\alpha = 1$ and $1/2$. The entropies start saturating to their maximum value. Small inset: Accumulated local truncation error of one site. Right: The same evolution as above, but now with a disorder strength $h = 2$ and for $d_A = 2$. The simulation time has been extended slightly compared to the clean case without disorder. One also notices a slow down in the growth of local Renyi entropies. The simulations are done for $\delta t = 0.1$ and 0.01 for $D = 4$ and $\delta t = 0.01$ for $D = 5$. The results are consistent with different Trotter sizes as well as different bond dimensions, building trust in our simulations.

the spectrum divided into blocks for the discrete disorder, the resulting IPRs are also much smaller than in the continuous case, indicating that these states are not localized. When including many-body interactions, these can be interpreted as additional on-site fields that depend on the particle configuration. This renders the potential experienced by the particles close to continuous restoring localization. We will explore this in the following section.

Results for interacting $\Delta = 1$ case

First, we will present the results for the clean case as well as the simplest case of disorder we can incorporate in our iPEPS simulations using the auxiliary method. The simplest case is with binary disorder when the auxiliary system has a local Hilbert space (d_A) of two implying that our disorder landscape has two levels locally. We start by computing the expectation value of the particle number as a function of real time. The expectation values are computed at the two different physical sites of the tensor network. Since the initial physical state is a Néel state, its expectation values are 1 for the occupied site and 0 at the empty site at $t = 0$. As we initiate the quench, we want to analyze how the particle number changes with time. This is closely related to the experimentally used *imbalance* [18,36,67], which measures the difference of particle occupation between even and odd sites. In the absence of any disorder, this imbalance will eventually drop to zero, or in other words, the particles will spread leading to a homogeneous particle distribution. This is shown in the left panel of Fig. 5, although the time scale has been cut off early to avoid errors, according to criteria specified below.

For the calculations, we have used an iPEPS with a fixed bond dimension $D = 4, 5$ and Trotter step of 0.1 and 0.01.

The reason for the comparably small bond dimension is that the physical dimension needs to be comparably large. The results for both the Trotter steps as well as different bond dimensions are depicted in Figs. 5 and 6. As with all other tensor network approaches, iPEPS cannot be used for long time simulations due to the rapid growth of entanglement [68,69], which can only be accounted for by (in time exponentially) large bond dimensions. This is a fundamental challenge that ultimately cannot be overcome for any universal classical simulation method, as Hamiltonian evolution is in principle as powerful as a quantum computer (is BQP complete in technical terms [70]), and hence a universal classical efficient method of local Hamiltonian evolution for all times is unlikely to exist [71]. Using large bond dimensions in two dimensions is significantly more challenging compared to the one-dimensional case and comes along with significant computational effort. As a consequence, the error measures must necessarily be less stringent here compared to the situation in one spatial dimension.

The main criterion that we make use of for stopping the time evolution is a disagreement of the two largest available PEPS bond dimensions (which would here be $D = 4$ and 5), reflecting a convergence in bond dimension: This convergence builds trust in the expectation that higher bond dimensions provide compatible results. This is shown in Figs. 5 and 6. Some further intuition is also provided by monitoring the growth of the local Renyi entropies in time starting from the initial product state. We compute the Renyi entropies $S(\rho_1)$ of order $\alpha = 1$ and $1/2$ for the reduced density matrix of one site. The scaling of Renyi entropies can be precisely related to tensor network state approximations in one spatial dimension [72]. Here, the issue at hand is more subtle, as we operate in two spatial dimensions, and observing entropies of
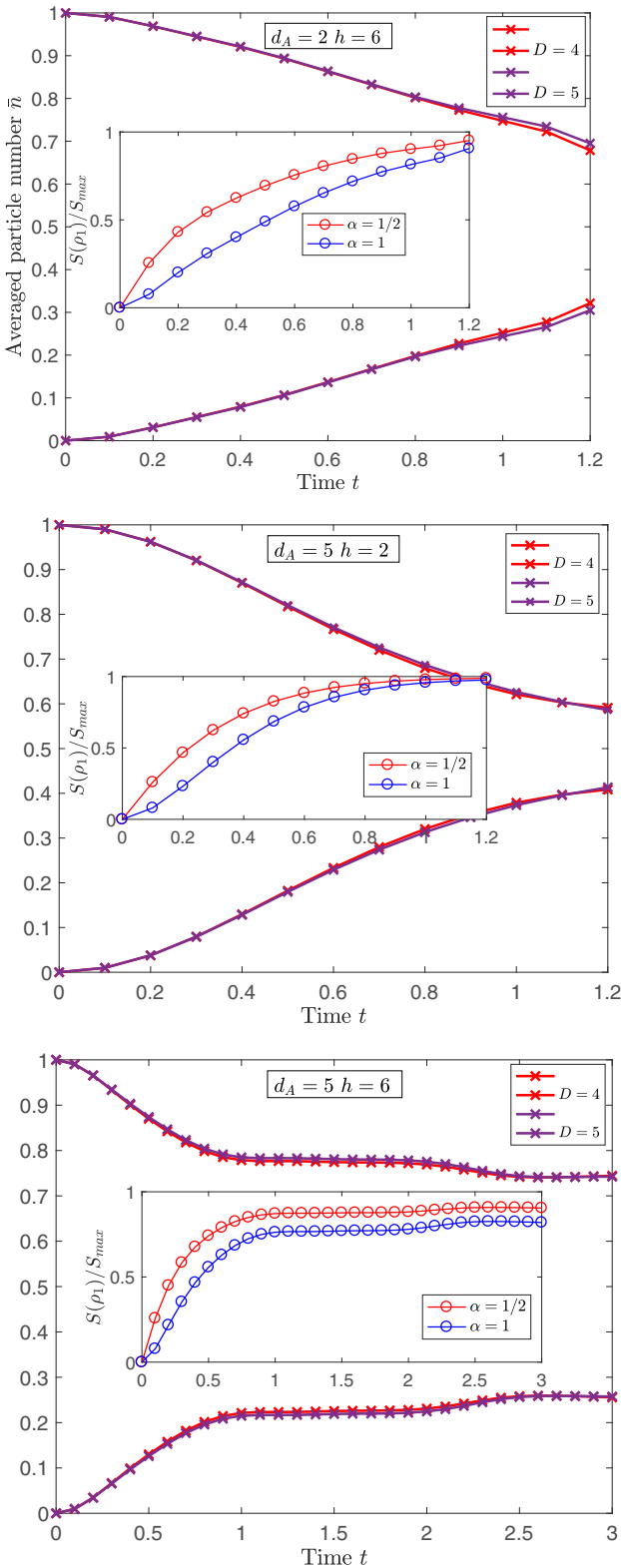
FIG. 6. Similar to Fig. 5 but for stronger disorder and more disorder levels. Top: Relatively strong disorder $h = 6$ but only two levels of disorder $d_A = 2$. Middle: More levels of disorder $d_A = 5$ but weak disorder strength $h = 2$. Bottom: Many disorder levels $d_A = 5$ as well as relatively strong disorder $h = 6$. In all the plots, we show simulations with bond dimensions $D = 4$ and 5 up to good agreement. This is also consistent with the growth of Renyi entropies, which are shown in the insets.

arbitrarily large reduced states is excessively challenging. Still, the deviation from a saturated value $S_{\max} = \ln(d_p)$, where d_p is the dimension of the local Hilbert space of the physical spins, can be seen as an indication that the tensor network approximation is still meaningful. We provide these numbers in the inset of Figs. 5 and 6. Furthermore, we show that our time evolution is stable against different Trotter steps $\delta t = 0.1$ and 0.01, which is a key insight in favor of the update scheme used here, as Ref. [27] convincingly discussed issues with stability with full updates. Along the way, we have also monitored the local truncation error to see that it is not significant for our purposes, again shown in the insets of Fig. 5. The local truncation error ϵ is the sum of the squares of discarded weights during the evolution for one site. For the case without disorder, we plot the results for up to $t = 0.8$, although $S(\rho_1)$ attains its maximal value at $t = 1$ hopping strength. The local truncation error is of the order of 10^{-4} until this time.

We now introduce disorder to our system. For a disorder strength of $h = 2$, we can see that the growth of entropy for a single site reduced density matrix slows down already, thereby allowing us to do time evolution to longer times. This is shown in the big inset of the right panel of Fig. 5. Just like the previous case, $S(\rho_1)$ in this case also becomes saturated after a few more time steps. The truncation error up to this time scale is of the order of 10^{-3} (shown in the small inset). Based on the particle number, there is still no strong indication of localization with such a weak disorder strength $h = 2$ and low levels of disorder $d_A = 2$. Increasing the bond dimension of the iPEPS will improve the simulation by a few time steps, but this is numerically very demanding. Similarly to the noninteracting case, we will investigate the influence of increasing the size of the local Hilbert space of the auxiliary system, thereby allowing more levels of disorder locally as well as the disorder strength.

We first increase the disorder strength for the binary disorder case reflected by $d_A = 2$. This is shown in the top panel of Fig. 6. There is no significant change compared to the case of $h = 2$ and $d_A = 2$. We now increase the number of levels of disorder in our system by increasing the local dimension of the Hilbert space of the auxiliary spins. We investigate this for $d_A = 3, 4, 5, 6$ and for different values of the disorder strengths $h = 2, 4, 6$. $d_A \to \infty$ corresponds to the case of continuous disorder. In Fig. 6, we only show the plots for $d_A = 2$, $h = 6$ (top); $d_A = 5$, $h = 2$ (middle); and $d_A = 5$, $h = 6$ (bottom). What we see from Fig. 6 is that merely increasing the disorder strength h or the number of disorder levels d_A alone is not sufficient to see signatures of localization, and ergodicity seems to be preserved, judging from dynamical data. Only in the case with relatively strong disorder $h = 6$ and many levels of disorder $d_A = 5$ available are clear signatures of localization encountered. As a consequence, we are able to go to much longer times in our simulation, $t = 3J$. We would like to note here that to the best of our knowledge, this is the longest time achieved in time evolution with 2D tensor networks in the thermodynamic limit, facilitated by features of localization. Signatures of localization are also reflected by the considerable slowdown of the growth of local Renyi entropies (as shown in the inset of the plots).
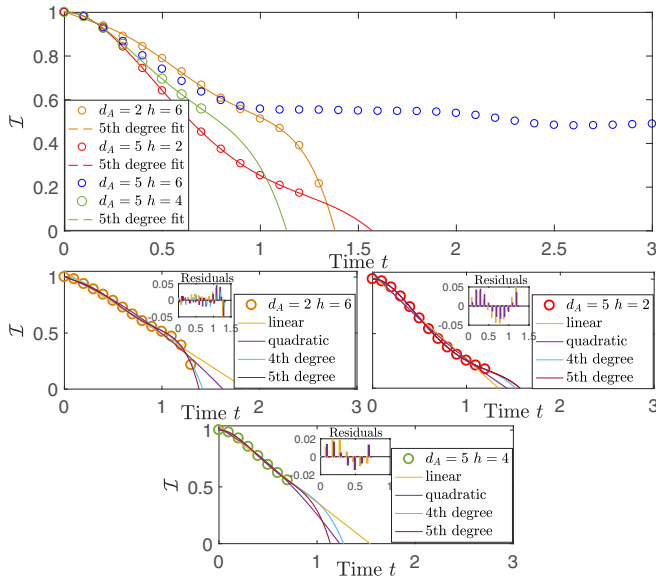
FIG. 7. Particle imbalance $\mathcal{I}$ for various configurations of disorder dimensions d_A and strengths h. We show the dynamics of the longest available times for the localized case (blue circles, $h = 6$ and $d_A = 5$), which is up to three hoppings. Also shown are the cases in which the particles do not localize (yellow circles with $h = 6$, $d_A = 2$, red circles with $h = 2$, $d_A = 5$, and green circles with $h = 4$, $d_A = 5$). The dynamics can be extrapolated using different polynomials such as linear, quadratic, fourth, and fifth degree fit, and one can notice the imbalance dropping to zero in all these cases. Also shown are the residuals corresponding to each fit (dashed lines). The linear fit has the largest error, while the fifth degree polynomial fits in this sense most accurately.

To be more comprehensive and systematic, we now consider different configurations of the disorder strength h and disorder levels d_A, and we plot the particle imbalance $\mathcal{I}$, defined as the difference in the occupation number of the two different sites. This is shown in Fig. 7 for the configurations $(d_A = 2, h = 6)$, $(d_A = 5, h = 2)$, $(d_A = 5, h = 4)$, and $(d_A = 5, h = 6)$. As we see, only in the last configuration can one go as far as achieving the longest time evolution, because only then does the system undergo localization reflected by slow dynamics up to this time. For the other situations, one has to be content with the available short time dynamics. To make predictions with a reliably statistical basis, we have nonetheless extrapolated these available times using different polynomial fits such as linear, quadratic, fourth, and fifth degree polynomial least-squares fits. This procedure allows for crude predictive statements on future behavior, and indeed, the particle imbalance in all these cases conveniently and convincingly drops to zero (reflecting no remaining imbalance). These are shown by dashed lines in Fig. 7 along with the residuals of their fit to be precise.

Based on the available information within the achievable times, we are now able to go a step further: Building on dynamical data, we can arrive at crude estimates of the phase diagram of many-body localization in 2D based on the disorder strength h and the levels of disorder d_A, judged from dynamical data. Even though these estimates are necessarily coarse-grained, it is still exciting to see that the approach
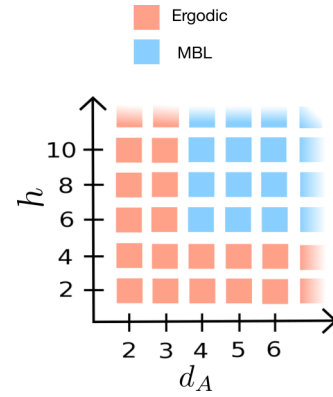

FIG. 8. Crude estimate of the phase diagram as being assessed from dynamical localization as a function of the disorder dimension d_A and the disorder strength h. The criterion to assign an ergodic or localized phase is whether the achievable simulation in time or the polynomial interpolation exhibits a localization of the imbalance in time. A disorder strength of $h = 6J$ with at least four levels of disorder seems necessary to give rise to many-body localization in 2D.

taken allows us to draw conclusions along these lines, in a regime that is very little studied using analytical and numerical state-of-the-art techniques. The results of this endeavor are shown in Fig. 8. Pink boxes indicate that the system is likely to thermalize and is therefore ergodic, while blue boxes indicate that the system localizes for the available time scales and is therefore in the MBL phase. This is a dynamical phase diagram available for 2D dynamics with discrete disorder. Our dynamical phase indicates that in order to achieve MBL in two spatial dimensions, one needs a critical disorder strength of $h = 6$ and disorder levels $d_A = 4$. The experimental work of Ref. [18] had found a critical disorder strength of $h = 5.5$ for continuous disorder in an Aubrey-Andre model, even though it is important to stress that the underlying Hamiltonian model is that of a two-dimensional Bose Hubbard model. A complementing theoretical work based on constructing cellular automata had found a critical disorder strength of $h = 19$, aimed again at exploring the disordered Bose-Hubbard model [25].

We have been able to find that while discrete disorder landscapes lead to no noticeable localization for the two-dimensional noninteracting systems we consider, they appear to be capable of localizing interacting systems. This is consistent with the argument given above that the interaction can be viewed as an additional source of randomness that depends on the adjacent particle configuration. It is also compatible with the rigorous findings [31–35] (as the disorder can be too small and the magnetization does not detect a finite correlation length), but it adds scope to this, as we discuss the impact of specific small auxiliary dimensions. Before all, our findings can be seen as an invitation to study in depth the rich physics of discrete disorder beyond one spatial dimension.

V. CONCLUSION AND OUTLOOK

We have studied the effect of disorder in two-dimensional systems using two independent techniques: a free fermionic

simulation for the noninteracting regime of the XXZ-Hamiltonian, and an iPEPS algorithm for the interacting regime. By implementing discrete levels of disorder in the latter case as well as continuous disorder for the free fermionic case, we have found strong numerical evidence for the many-body localization in infinite two-dimensional systems when using a sufficient number of disorder levels as well as disorder strength. Based on the dynamics of the particle imbalance for the available times, we have estimated a crude phase diagram of MBL in 2D, finding the critical disorder strength to $h = 6$ and at least four levels of disorder $d_A = 4$. Surprisingly, we do not find any evidence of localization for the infinite two-dimensional system for the noninteracting case using discrete levels of disorder, despite the mathematical proof of Anderson localization in two spatial dimensions with continuous disorder. We have provided an intuitive argument for why this is the case based on a decoupling of potential levels, which leads to an effective hopping problem, one that is also compatible with the findings of Ref. [31]. Our argument is supported by strong numerical evidence based on two independent techniques.

We argue that the significance of our work is fourfold: We present a stable numerical machinery that is able to explore a regime of disordered lattice models in higher dimensions that has formerly been significantly less accessible. Our machinery is more resource-efficient, stable, and provides better control over the dynamics. For this reason, we have been able to go to the longest available time scale of $t = 3J$ in 2D, thanks to the disorder. This is a technical, algorithmic improvement.

Then, we are able to freshly explore the physics of discrete disorder [31], a regime that we think has received less attention in the literature than it deserves, giving the rich interplay of discreteness of disorder and interactions, and only very recently has moved into the focus of attention in the Anderson, i.e., noninteracting, case [32–35]. It would be very interesting to understand the interplay of discrete disorder also in view of the stability of MBL and Griffiths effects.

Excitingly, our tools are powerful enough to provide some estimates of the phase diagram of many-body localization assessed by investigating dynamical properties, even though these estimates are necessarily crude for the time scales available. In light of the enormous difficulty of achieving such estimates, for example with quantum cellular automata [25], we think that our dynamical method provides some handle on studying the precise interplay and a phase diagram of the disorder strength and the number of levels of disorder with the system. The tools laid out here can be seen as an invitation to quantitatively study this interesting regime more thoroughly.

Finally, and maybe most importantly in the medium to long term, we are able to provide benchmarks for *quantum simulators* [73,74] that are increasingly becoming available in a number of physical platforms. With the advent of programmable randomness, this work can actually be probed directly in experiments as well. As mentioned before, the programmable nature allows us to avoid rare events of small local disorder and ergodic bubbles leading to a potential instability [22,23] as a design principle for choosing disorder patterns. For example, the programmable, reconfigurable arrays of individually *trapped cold atoms* with strong, coherent interactions realized by excitation to Rydberg states [75] give

rise to such a platform. In systems of *trapped ions* [76] and in *superconducting devices* [20], large degrees of flexibility arise in programming potentials in one spatial dimension, settings in which discrete disorder can be explored. Even beyond programmability, the presence of one—say, fermionic—atomic species constituting *discrete disorder for another atomic species* [77,78] opens up interesting perspectives.

Our work constitutes a basis on which a compelling conclusion can be drawn for the perspective of realizing such programmable quantum simulators from a complementing perspective: By further developing and applying tensor network techniques, we have entered an unprecedented regime for classical simulation techniques concerning the dimensionality of the system, the way disorder is realized, and at the same time concerning the times reached. This information can be made use of to build trust in the correctness of an eventual programmable quantum simulation in the sense of a partial *certification* [79] of the quantum simulation. This will work for comparably short times—for long times, no classical efficient computation will be able to keep track of the quantum dynamics [70,71]. To access such long times, one actually has to perform the quantum simulation in the laboratory, based on and guided by the insight provided by the classical simulation. In this sense, our work can be viewed as a blueprint for a programmable quantum simulation using near-term quantum devices that accesses an intricate quantum phase of matter. It is our hope that the present work will stimulate such endeavors.

APPENDIX

In this work, we use exact diagonalization (ED) and tensor network methods. For the case of a noninteracting system, we use ED up to system size 40×40. For the interacting system, we use infinite projected entangled paired states combined with the quantum dilation technique discussed in the main text, directly in the thermodynamic limit. For optimizing the tensors, we use the simple update scheme originally introduced for ground-state calculations [61]. The reasoning for choosing this scheme over the full update has been discussed in the main text already. For the update procedure, we use iPEPS with bond dimensions $D = 4$ and 5 with *Trotter* steps $\delta t = 0.1$ and 0.01. The combined dimensions of the physical

and the auxiliary spins used in these simulations are $d = d_p \times d_A = 4, 6, 8,$ and 10.

Once the tensors are optimized, we use the CTMRG technique [62,63,80,81] to contract the full environment of the tensors, thus targeting the thermodynamic limit. The CTMRG algorithm computes the effective environment of a particular site by contracting the whole infinite 2D lattice except the site at which we want to compute the observables. For this, one needs to obtain a set of fixed point tensors that makes up this effective environment. Details on how we do this can be found in Refs. [62,63,82]. The bond dimensions of the environment used are at least the square of the bond dimension of the iPEPS ($\chi \geqslant D^2$) and are sufficiently well-converged. The agreement between the expectation values of the highest available bond dimensions is used as one of the criteria for stopping our time evolution.

[1] J. Eisert, M. Friesdorf, and C. Gogolin, Quantum many-body systems out of equilibrium, Nat. Phys. **11**, 124 (2015).

[2] A. Polkovnikov, K. Sengupta, A. Silva, and M. Vengalattore, Non-equilibrium dynamics of closed interacting quantum systems, Rev. Mod. Phys. **83**, 863 (2011).

[3] C. Gogolin and J. Eisert, Equilibration, thermalisation, and the emergence of statistical mechanics in closed quantum systems, Rep. Prog. Phys. **79**, 056001 (2016).

[4] D. M. Basko, I. L. Aleiner, and B. L. Altshuler, Metal-insulator transition in a weakly interacting many-electron system with localized single-particle states, Ann. Phys. **321**, 1126 (2006).

[5] D. A. Abanin, E. Altman, I. Bloch, and M. Serbyn, Colloquium: Many-body localization, thermalization, and entanglement, Rev. Mod. Phys. **91**, 021001 (2019).

[6] A. Pal and D. A. Huse, The many-body localization transition, Phys. Rev. B **82**, 174411 (2010).

[7] R. Vosk, D. A. Huse, and E. Altman, Theory of the Many-Body Localization Transition in One-Dimensional Systems, Phys. Rev. X **5**, 031032 (2015).

[8] M. Goihl, M. Gluza, C. Krumnow, and J. Eisert, Construction of exact constants of motion and effective models for many-body localized systems, Phys. Rev. B **97**, 134202 (2018).

[9] M. Serbyn, Z. Papić, and D. A. Abanin, Universal Slow Growth of Entanglement in Interacting Strongly Disordered Systems, Phys. Rev. Lett. **110**, 260601 (2013).

[10] J. H. Bardarson, F. Pollmann, and J. E. Moore, Unbounded Growth of Entanglement in Models of Many-Body Localization, Phys. Rev. Lett. **109**, 017202 (2012).

[11] M. Znidaric, T. Prosen, and P. Prelovsek, Many-body localization in the Heisenberg XXZ magnet in a random field, Phys. Rev. B **77**, 064426 (2008).

[12] J. Eisert and T. J. Osborne, General Entanglement Scaling Laws from Time Evolution, Phys. Rev. Lett. **97**, 150404 (2006).

[13] M. C. Bañuls, N. Y. Yao, S. Choi, M. D. Lukin, and J. I. Cirac, Dynamics of quantum information in many-body localized systems, Phys. Rev. B **96**, 174201 (2017).

[14] M. Friesdorf, A. H. Werner, M. Goihl, J. Eisert, and W. Brown, Local constants of motion imply information propagation, New J. Phys. **17**, 113054 (2015).

[15] J. Eisert, M. Cramer, and M. B. Plenio, Area laws for the entanglement entropy, Rev. Mod. Phys. **82**, 277 (2010).

[16] B. Bauer and C. Nayak, Area laws in a many-body localised state and its implications for topological order, J. Stat. Mech. (2013) P09005.

[17] M. Friesdorf, A. H. Werner, W. Brown, V. B. Scholz, and J. Eisert, Many-Body Localisation Implies that Eigenvectors are Matrix-Product States, Phys. Rev. Lett. **114**, 170505 (2015).

[18] J.-Y. Choi *et al.*, Exploring the many-body localization transition in two dimensions, Science **352**, 1547 (2016).

[19] J. Smith *et al.*, Many-body localization in a quantum simulator with programmable random disorder, Nat. Phys. **12**, 907 (2016).

[20] P. Roushan *et al.*, Spectral signatures of many-body localization with interacting photons, Science **358**, 1175 (2017).

[21] A. Lukin *et al.*, Probing entanglement in a many-body-localized system, Science **364**, 256 (2019).

[22] W. De Roeck and F. Huveneers, Stability and instability towards delocalization in many-body localization systems, Phys. Rev. B **95**, 155129 (2017).

[23] W. D. Roeck and J. Z. Imbrie, Many-body localization: Stability and instability, Philos. Trans. R. Soc. London, Ser. A **375**, 20160422 (2017).

[24] A. Geißler and G. Pupillo, Many-body localization in the two dimensional Bose-Hubbard model, Phys. Rev. Research **2**, 042037(R) (2020).

[25] T. B. Wahl, A. Pal, and S. H. Simon, Signatures of the many-body localized regime in two dimensions, Nat. Phys. **15**, 164 (2019).

[26] M. D. Kennes, Many-body localization in two dimensions from projected entangled-pair states, arXiv:1811.04126.

[27] C. Hubig and J. I. Cirac, Time-dependent study of disordered models with infinite projected entangled pair states, SciPost Phys. **6**, 31 (2019).

[28] G. De Tomasi, F. Pollmann, and M. Heyl, Efficiently solving the dynamics of many-body localized systems at strong disorder, Phys. Rev. B **99**, 241114(R) (2019).

[29] F. Andraschko, T. Enss, and J. Sirker, Purification and Many-Body Localization in Cold Atomic Gases, Phys. Rev. Lett. **113**, 217201 (2014).

[30] B. Paredes, F. Verstraete, and J. I. Cirac, Exploiting Quantum Parallelism to Simulate Quantum Random Many-Body Systems, Phys. Rev. Lett. **95**, 140501 (2005).

[31] R. Carmona, A. Klein, and F. Martinelli, Anderson localization for bernoulli and other singular potentials, Commun. Math. Phys. **108**, 41 (1987).

[32] J. Z. Imbrie, Localization and eigenvalue statistics for the lattice anderson model with discrete disorder, arXiv:1705.01916.

[33] S. D. Bievre and F. Germinet, Dynamical localization for the random dimer schrödinger operator, J. Stat. Phys. **98**, 1135 (2000).

[34] J. Ding and C. K. Smart, Localization near the edge for the anderson bernoulli model on the two dimensional lattice, arXiv:1809.09041.

[35] L. Li and L. Zhang, Anderson-bernoulli localization on the 3d lattice and discrete unique continuation principle, arXiv:1906.04350.

[36] S. Trotzky *et al.*, Probing the relaxation towards equilibrium in an isolated strongly correlated one-dimensional Bose gas, Nat. Phys. **8**, 325 (2012).

[37] D. Abanin, W. De Roeck, W. W. Ho, and F. Huveneers, A rigorous theory of many-body prethermalization for periodically driven and closed quantum systems, Commun. Math. Phys. **354**, 809 (2017).

[38] J. Suntajs, J. Bonca, T. Prosen, and L. Vidmar, Quantum chaos challenges many-body localization, arXiv:1905.06345.

[39] M. Goihl, N. Walk, J. Eisert, and N. Tarantino, Harnessing symmetry-protected topological order for quantum memories, Phys. Rev. Res. **2**, 013120 (2020).

[40] F. Verstraete and J. I. Cirac, Renormalization algorithms for quantum-many body systems in two and higher dimensions, arXiv:cond-mat.040706.

[41] F. Verstraete, M. M. Wolf, D. Perez-Garcia, and J. I. Cirac, Criticality, the Area Law, and the Computational Power of Projected Entangled Pair States, Phys. Rev. Lett. **96**, 220601 (2006).

[42] R. Orús, A practical introduction to tensor networks: Matrix product states and projected entangled pair states, Ann. Phys. **349**, 117 (2014).

[43] F. Verstraete, J. I. Cirac, and V. Murg, Matrix product states, projected entangled pair states, and variational renormalization group methods for quantum spin systems, Adv. Phys. **57**, 143 (2008).

[44] J. Eisert, Entanglement and tensor network states, arXiv:1308.3318.

[45] J. Jordan, R. Orus, G. Vidal, F. Verstraete, and J. I. Cirac, Classical Simulation of Infinite-Size Quantum Lattice Systems in Two Spatial Dimensions, Phys. Rev. Lett. **101**, 250602 (2008).

[46] P. Corboz, T. M. Rice, and M. Troyer, Competing States in the t-j Model: Uniform d-Wave State Versus Stripe State, Phys. Rev. Lett. **113**, 046402 (2014).

[47] H. J. Liao, Z. Y. Xie, J. Chen, Z. Y. Liu, H. D. Xie, R. Z. Huang, B. Normand, and T. Xiang, Gapless Spin-Liquid Ground State in the $s = 1/2$ Kagome Antiferromagnet, Phys. Rev. Lett. **118**, 137202 (2017).

[48] T. Picot, M. Ziegler, R. Orús, and D. Poilblanc, Spin-s kagome quantum antiferromagnets in a field with tensor networks, Phys. Rev. B **93**, 060407(R) (2016).

[49] A. Kshetrimayum, T. Picot, R. Orús, and D. Poilblanc, Spin-$\frac{1}{2}$ kagome XXZ model in a field: Competition between lattice nematic and solid orders, Phys. Rev. B **94**, 235146 (2016).

[50] Y. H. Matsuda *et al.*, Magnetization of $srcu_2(bo_3)_2$ in Ultrahigh Magnetic Fields up to 118 t, Phys. Rev. Lett. **111**, 137204 (2013).

[51] P. Corboz and F. Mila, Crystals of Bound States in the Magnetization Plateaus of the Shastry-Sutherland Model, Phys. Rev. Lett. **112**, 147203 (2014).

[52] A. Kshetrimayum, C. Balz, B. Lake, and J. Eisert, Tensor network investigation of the double layer kagome compound ca10cr7o28, Ann. Phys. **421**, 168292 (2020).

[53] P. Czarnik, L. Cincio, and J. Dziarmaga, Projected entangled pair states at finite temperature: Imaginary time evolution with ancillas, Phys. Rev. B **86**, 245101 (2012).

[54] P. Czarnik and J. Dziarmaga, Variational approach to projected entangled pair states at finite temperature, Phys. Rev. B **92**, 035152 (2015).

[55] A. Kshetrimayum, M. Rizzi, J. Eisert, and R. Orús, Tensor Network Annealing Algorithm for Two-Dimensional Thermal States, Phys. Rev. Lett. **122**, 070502 (2019).

[56] S. Mondal, A. Kshetrimayum, and T. Mishra, Two-body repulsive bound pairs in a multi-body interacting Bose-Hubbard model, Phys. Rev. A **102**, 023312 (2020).

[57] A. Kshetrimayum, H. Weimer, and R. Orus, A simple tensor network algorithm for two-dimensional steady states, Nat. Commun. **8**, 1291 (2017).

[58] H. Weimer, A. Kshetrimayum, and R. Orús, Simulation methods for open quantum many-body systems, arXiv:1907.07079.

[59] P. Czarnik, J. Dziarmaga, and P. Corboz, Time evolution of an infinite projected entangled pair state: An efficient algorithm, Phys. Rev. B **99**, 035115 (2019).

[60] T. Enss, F. Andraschko, and J. Sirker, Many-body localization in infinite chains, Phys. Rev. B **95**, 045121 (2017).

[61] H. C. Jiang, Z. Y. Weng, and T. Xiang, Accurate Determination of Tensor Network State of Quantum Lattice Models in Two Dimensions, Phys. Rev. Lett. **101**, 090603 (2008).

[62] R. Orús, Exploring corner transfer matrices and corner tensors for the classical simulation of quantum lattice systems, Phys. Rev. B **85**, 205117 (2012).

[63] R. Orús and G. Vidal, Simulation of two-dimensional quantum systems on an infinite lattice revisited: Corner transfer matrix for tensor contraction, Phys. Rev. B **80**, 094403 (2009).

[64] W. Kirsch, An Invitation to random Schroedinger operators, arXiv:0709.3707.

[65] G. Stolz, An introduction to the mathematics of Anderson localization, in *Entropy and the Quantum II*, Vol. 552 of *Contemp. Math.* (Am. Math. Soc., University of Arizona, 2011).

[66] D. Hundertmark, A short introduction to Anderson localization. in *Proceedings of the LMS Meeting on Analysis and Stochastics of Growth Processes and Interface Models* (Oxford University Press, Oxford, 2007).

[67] M. Cramer, A. Flesch, I. P. McCulloch, U. Schollwöck, and J. Eisert, Exploring Local Quantum Many-Body Relaxation by Atoms in Optical Superlattices, Phys. Rev. Lett. **101**, 063001 (2008).

[68] N. Schuch, M. M. Wolf, K. G. H. Vollbrecht, and J. I. Cirac, On entropy growth and the hardness of simulating time evolution, New J. Phys. **10**, 033032 (2008).

[69] M. Cramer, C. M. Dawson, J. Eisert, and T. J. Osborne, Quenching, Relaxation, and a Central Limit Theorem for Quantum Lattice Systems, Phys. Rev. Lett. **100**, 030602 (2008).

[70] K. G. H. Vollbrecht and J. I. Cirac, Quantum Simulators, Continuous-Time Automata, and Translationally Invariant Systems, Phys. Rev. Lett. **100**, 010501 (2008).

[71] M. L. Baez, M. Goihl, J. Haferkamp, J. Bermejo-Vega, M. Gluza, and J. Eisert, Dynamical structure factors of dynamical quantum simulators, Proc. Natl. Acad. Sci. (USA) **117**, 26123 (2020).

[72] N. Schuch, M. M. Wolf, F. Verstraete, and J. I. Cirac, Entropy Scaling and Simulability by Matrix Product States, Phys. Rev. Lett. **100**, 030504 (2008).

[73] I. Bloch, J. Dalibard, and S. Nascimbene, Quantum simulations with ultracold quantum gases, Nat. Phys. **8**, 267 (2012).

[74] J. I. Cirac and P. Zoller, Goals and opportunities in quantum simulation, Nat. Phys. **8**, 264 (2012).

[75] H. Bernien *et al.*, Nature (London) **551**, 579 (2017).

[76] S. Debnath *et al.*, Demonstration of a small programmable quantum computer with atomic qubits, Nature (London) **536**, 63 (2016).

[77] V. Ahufinger, L. Sanchez-Palencia, A. Kantian, A. Sanpera, and M. Lewenstein, Disordered ultracold atomic gases in optical lattices: A case study of Fermi-Bose mixtures, Phys. Rev. A **72**, 063616 (2005).

[78] A. Mering and M. Fleischhauer, One-dimensional Bose-Fermi-Hubbard model in the heavy-fermion limit, Phys. Rev. A **77**, 023601 (2008).

[79] J. Eisert *et al.*, Quantum certification and benchmarking, Nat. Rev. Phys. **2**, 382 (2020).

[80] T. Nishino and K. Okunishi, Corner transfer matrix renormalization group method, J. Phys. Soc. Jpn. **65**, 891 (1996).

[81] T. Nishino and K. Okunishi, Corner transfer matrix algorithm for classical renormalization group, J. Phys. Soc. Jpn. **66**, 3040 (1997).

[82] A. Kshetrimayum, Quantum many-body systems and tensor network algorithms. Ph.D. thesis, Johannes Gutenberg-Universität Mainz (2017).